Topics in Catalysis (2021) 64:36–50
https://doi.org/10.1007/s11244-020-01355-3

ORIGINAL PAPER

Selective Photo-epoxidation of (R)-(+)- and (S)-(−)-Limonene by Chiral and Non-Chiral Dioxo-Mo$^{(VI)}$ Complexes Anchored on TiO_2-Nanotubes

Henry Martínez Q.[1] · **Edgar A. Paez-Mozo**[1] · **Fernando Martínez O.**[1]

Published online: 19 August 2020

Abstract

Selective epoxidation of the (R) and (S) isomers of limonene by dioxomolybdenum$^{(VI)}$ complexes anchored covalently on TiO_2 nanotubes using UV–Vis light and O_2 as the oxidizing agent was evaluated. It is interesting to study the effect of the ligands: bipyridine, terpyridine, and Schiff base on the stereoselective epoxidation of limonene through photostimulated oxygen atom transfer (OAT). OAT activity observed to increase in the following order: $Mo^{(VI)}O_2$(Schiff base)/TiO_2-NT < $Mo^{(VI)}Cl_2O_2$ (bipyridine)/TiO_2-NT < $Mo^{(VI)}Cl_2O_2$(terpyridine)/TiO_2-NT. Moderate diastereoselectivity to the *cis*-isomer of complexes with "non-chiral" ligands like bipyridine and terpyridine was displayed. Contrary to the complex with the Schiff base as "chiral" ligand, it showed an increase in diastereoisomeric excess (52%), associated to an asymmetric double induction, assuming a complex metal-oxo sideway interaction with the trisubstituted olefins at the transition state.

Graphic Abstract

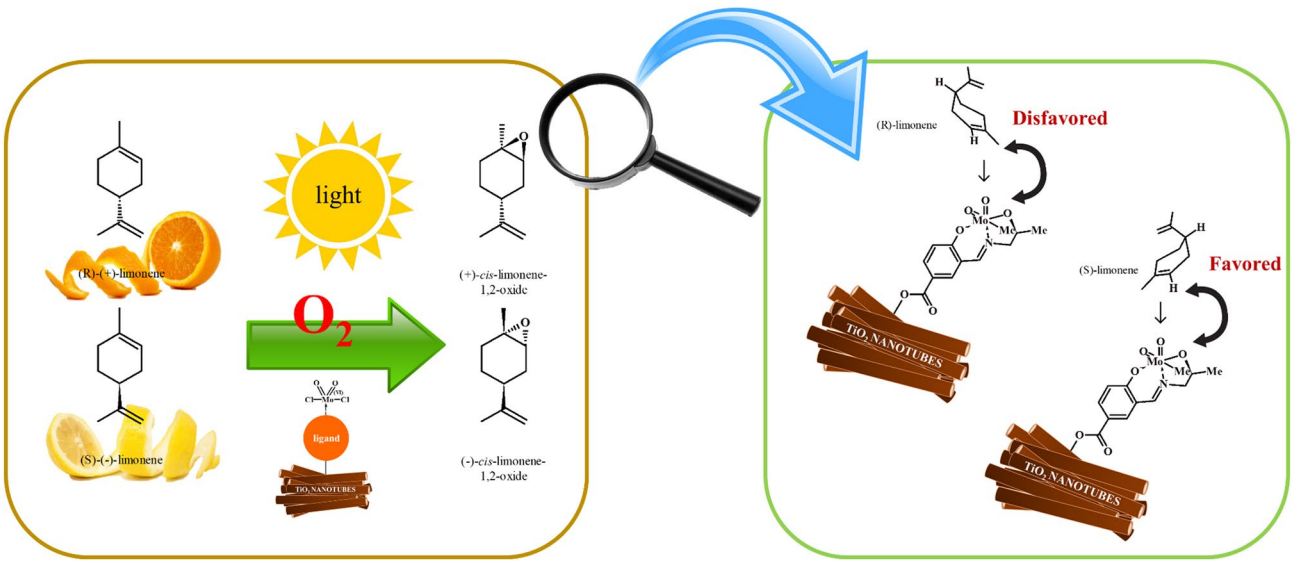

Keywords Diastereoselective epoxidation · Molybdenum complexes · Schiff base ligands · Bipyridine ligands · Terpyridine ligands · Oxygen atom transfer

Electronic supplementary material The online version of this article (https://doi.org/10.1007/s11244-020-01355-3) contains supplementary material, which is available to authorized users.

✉ Fernando Martínez O.
fmartine@uis.edu.co

Extended author information available on the last page of the article

1 Introduction

The preparation of chiral epoxides is interesting in order to obtain the building blocks for organic synthesis, including the production of drugs, biologically active compounds,

agricultural chemicals, and materials. Development of the organometallic enantioselective catalysis has been one of the most important hits of the last century, allowing the transformation of prochiral and racemic substrates into enantioenriched products [1, 2]. Limonene oxide is a valued bio-based building block in asymmetric synthesis and used as a chiral precursor of fragrances, perfumes, and food additives mainly [3, 4].

Figure 1 shows the variety of products of oxidation of (R)- and (S)-limonene (epoxides, carvone, carveol) that are obtained. Epoxides can be synthesized by oxidation at either one or both 1, 2, and 8, 9 double bonds. Furthermore, two types of diastereomers (*cis* and *trans*) are expected for each of the epoxide products. Typically, *cis*/*trans* diastereomers are formed in a racemic mixture [5–7].

At present, one of the challenges at level industrial and environmental is to design a highly active process, inducing full control over chemo-, regio- and stereoselectivity, decreasing by-products and allowing catalyst recycling. Olefinic bonds are relatively inert functionalities requiring chemical modification (functionalization) before use in fine chemical synthesis. The first examples of enantioselective epoxidation (allylic alcohols) were reported in 1977 using chiral molybdenum and vanadium complexes as catalysts, and alkyl hydroperoxides as terminal oxidants. Since the early 1980s, numerous catalyst systems have appeared, relying on either transition metal-based or purely organic. The catalyst most recognized were Katsuki's and Jacobsen's manganese–Salen systems for the epoxidation of unfunctionalized olefins [8, 9].

Several homogeneous and heterogeneous catalytic systems have performed limonene epoxidation. Chiral and achiral Jacobsen's catalysts in solution or immobilized on Al-MCM-41 exhibit similar conversion (60–80%), selectivity to a 1, 2-limonene epoxide (70–90%) and diastereoisomeric excess (d.e.) (20–50%) during diastereoselective epoxidation of limonene when in situ generated dimethyldioxirane used as an oxidizing agent, is in situ generated [5]. Homogeneous limonene epoxidation has also been performed by chloroperoxidase (CPO) from *Caldariomyces fumago* that catalyzes different reactions like hydroxylation and epoxidation of olefins with high yields and enantiomeric excess (ee) [10].

Heterogeneous catalysts have also displayed activity in limonene epoxidation reactions. Heteropolyacids anchored on Amberlite IRA-900 with hydrogen peroxide as the oxidant was used. However, epoxide obtained poisons the catalyst and inhibits the reaction at about 160 turnovers [11]. Mn–Salen complexes catalysts anchored on MCM-41 indicated moderate conversion (50–80%), but a low selectivity to limonene epoxide (< 20%) using *t*-BHP as oxidant [12]. With a chiral complex of sulfonato manganese (Salen) intercalated into a Zn(II)–Al(III) lamellar double hydroxide using molecular oxygen, gives 100% conversion, 93% epoxide selectivity and 43% diastereoisomeric excess at room temperature [13]. Manganese(Salen) catalysts supported on silica with H_2O_2 as the oxygen donor produced a yield up 80% at 24 h reaction. Another manganese(Salen) complex immobilized

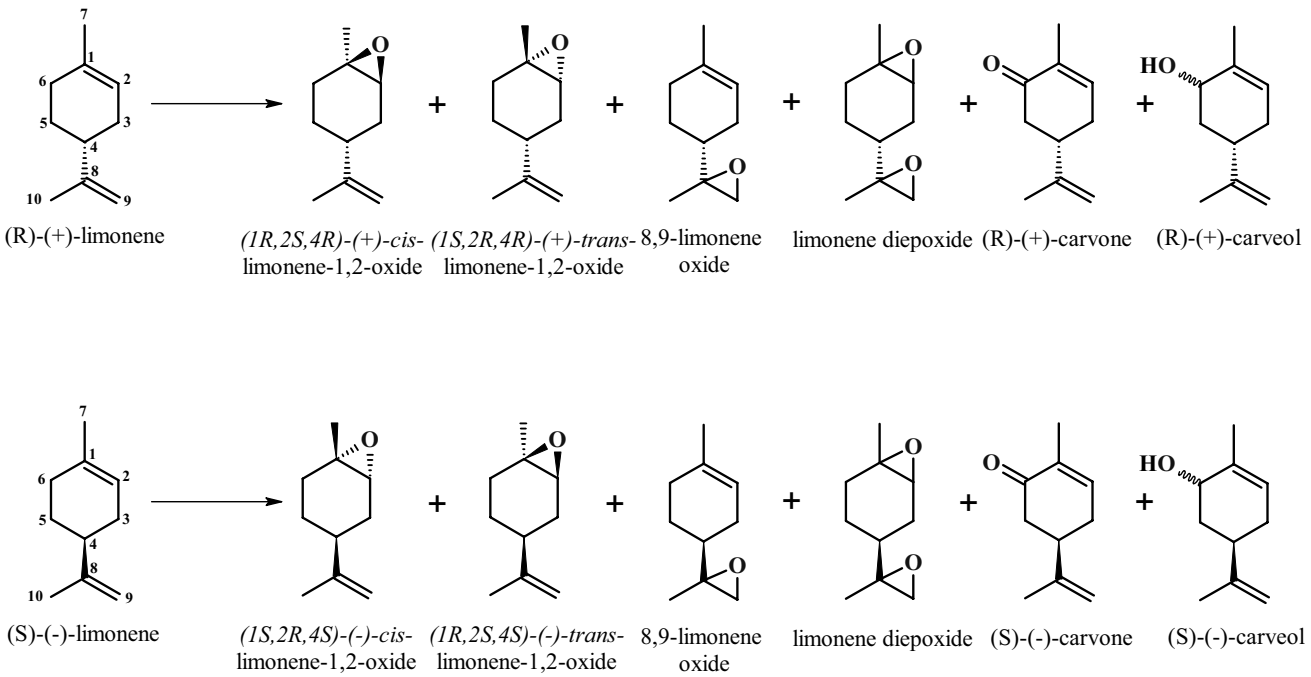

Fig. 1 Chemical structure of the possible limonene oxidation products

on SBA-15 [14] molecular sieves or zeolite-Y with atmospheric oxygen at 25 °C had given diastereoisomeric excess up 39%. In the case of manganese(Salen) supported on the ion-exchange resin (Dowex MsCl PW-Amberlite) used as a catalyst in the limonene epoxidation with sodium periodate and hydrogen peroxide attained an 85% of conversion and a 55% of epoxide selectivity at room temperature [15]. In contrast, cross-linked polystyrene resin as support of manganese porphyrin used in limonene epoxidation by sodium periodate attaining a 70% of conversion and a 35% epoxide selectivity at 3 h reaction [16]. Finally, limonene catalytic epoxidation with Co/SBA-16 [17] using O_2 as oxidant and isobutyraldehyde as a reductant presented a high conversion (99%) and a selectivity (50%) into 1,2-limonene oxide and limonene dioxide (33%) respectively.

Different oxo- and dioxo-molybdenum complexes as oxygen atom transfer (OAT) catalysts have been evaluated in selective limonene oxidation. A dioxomolybdenum$^{(VI)}$ compound anchored on mesoporous silica (MCM-41) with *t*-BuOOH permitted a 75% conversion and about 90% epoxide selectivity at 55 °C and 7 h reaction [18]. Oxo molybdenum complexes containing chiral oxazolines with diastereoselectivity was tested in the epoxidation of limonene. However, using oxazolinyl-pyridine ligands favors the diastereoselectivity of trans-1,2-epoxide (*trans*/*cis*: 90/10) for the (R)-limonene epoxidation [1]. Also, dioxomolybdenum complexes with *t*-BuOOH as an oxygen donor presented an epoxide selectivity of 47% at 55 °C. In contrast, manganese(Salen) complex with iodosylbenzene or sodium hypochlorite gives up 90% of conversion but low selectivity to epoxides. Recently, the use of ionic liquid instead of organic solvent has allowed the exclusive formation of the *trans* epoxide [19].

Likewise, Jacobsen's Schiff-base complexes have been recognized as outstanding catalysts for the asymmetric epoxidation of *cis* substituted olefin unfunctionalized as cyclic dienes or polyenes, but still not used for limonene epoxidation. Another system formed by a molybdenum complex anchored a mesoporous nanocomposite material comprising helical chiral channels and with embedded magnetic iron oxide nanoparticles in the Si-MCM-41 type framework in the (R)-limonene epoxidation under air was assayed. Stereoselectivity observed was about 70–74% using decane as solvent at 393 K. The performance in asymmetric catalysis was found to be outstanding across a set of olefins. It observed that the helical channel has a positive influence on the diastereoselectivity of the catalytic epoxidation of different substrates [20].

We studied the selective catalytic oxidation of olefins with bipyridine-based Mo$^{(VI)}$ complexes grafted on TiO_2 different supports [21–24]. This heterogeneous system had been used in the catalytic epoxidation of monoterpenes like α-pinene [25]. Previously has been reported that the introduction of donor ligand drove to Mo$^{(VI)}$ compounds to catalyst highly selective oxidations of large organic molecules [26]. The present work has studied the effect of dioxomolybdenum$^{(VI)}$ complexes with chiral and nonchiral ligands like bipyridine, terpyridine, and Schiff base covalently anchored on TiO_2 nanotubes on the selective epoxidation of (R)-and (S)-limonene to produce the diastereoselective *cis*-isomer.

2 Experimental

2.1 Materials and Reagents

TiO_2 (anatase nanopowder, Sigma-Aldrich), NaOH (Merck), MoO_2Cl_2 (Sigma-Aldrich), $MoO_2(acac)_2$ (Sigma-Aldrich), bis(trimethylsilyl)urea (98%, Alfa Aesar), 2,2′-bipyridine-4,4′-dicarboxylic acid (98%, Sigma-Aldrich), (S)-(+)-1-amino-2-propanol (98%, Alfa Aesar), 3-formyl-4-hydroxybenzoic acid (97%, Sigma-Aldrich), 2,2′:6′,2″-terpyridine-4′-carboxylic acid (%, Alfa-Aesar) (R)-(+)-limonene (98%, Alfa Aesar), (S)-(−)-limonene (98%, Alfa Aesar) and other reagents were obtained from commercial sources and were used as received. Acetonitrile was bubbled with N_2 before use in each reaction. All complexes preparations and manipulations were carried out under oxygen- and water-free argon atmosphere using standard Schlenk techniques.

2.2 Instrumentation

The TiO_2-NT support was characterized by powder X-ray diffraction (XRD) using a Bruker AXS D8 Advance with monochromatized Cu Kα radiation (λ = 1.5418 Å) at 40 kV and 30 mA. The diffraction pattern was recorded at 2θ value range (20°–70°) with a step size of 0.01° and a step time of 0.4 s. The morphology of the support was characterized by TEM (Tecnai 183 F20 Super Twin TMP). Nitrogen adsorption–desorption isotherms at − 196 °C were obtained using a Micromeritics 3Flex apparatus. Before analysis, samples were degassed under vacuum at 110 °C for 8 h. The specific surface area was determined from the linear part (0–0.23 P/P_0) of the BET plot. The pore size distribution was determined by the BJH method applied to the adsorption branch. Raman spectra were obtained using a Raman Confocal Microscope (LabRAM HR Evolution HORIBA Scientific), irradiated with a laser of wavelength 532 nm, 10 mW output power, 10× objective, integration time 2 s and 10 accumulations. IR analysis was performed on a Bruker Tensor 27. UV–Vis diffuse reflectance spectroscopy used to determine bandgap energy (Shimadzu UV 2401PC). ^{13}C CP-MAS NMR analyzes were measured on a Bruker NMR spectrometer Advance 400 MHz, operating at a resonance frequency of 101.6 MHz for ^{13}C. The amount of anchored

$Mo^{(VI)}O_2Ln$ complex was determined by thermogravimetric analyzed (TGA) under N_2 atmosphere from 25 to 800 °C with a heating rate of 10 °C min^{-1}. The molybdenum content of complex was determined by atomic absorption spectroscopy using a Thermo S Series spectrometer. The sample digestion was performed with a mixture of hydrochloric and perchloric acid for 4 h.

2.3 $Mo^{(VI)}O_2Ln/TiO_2$-NT Catalysts Preparation

2.3.1 TiO_2 Nanotubes Preparation

TiO_2 nanotubes were prepared according to a previously reported alkaline hydrothermal methodology [25, 27] with some modifications using TiO_2 nanopowder (Aldrich) as the precursor.

2.3.2 Ligands Silylation

Ligands silylation was made according to a previous reported methodology [28]. Bis(trimethylsilyl)urea (1 mmol) was added to a CH_2Cl_2 solution (40 mL) containing respective ligand (1 mmol), and the mixture was refluxed for 6 h. The resulting suspension was filtered, and the filtrate evaporated cautiously in vacuum.

2.3.3 $MoCl_2O_2$(4,4′-dicarboxytrimethylsilyl-2,2′-bipyridine)

A benzene solution (40 mL) containing bis(trimethylsilyl)-2,2′-bipyridine-4,4′-dicarboxylate (1 mmol, previously prepared) was added to a benzene suspension (20 mL) containing MoO_2Cl_2 (1 mmol). The mixture was stirred for 4 h at room temperature resulting in a clear solution. Evaporation of the solvent yielded a white solid.

2.3.4 $MoCl_2O_2$[trimetilsilil[2,2′:6′,2″-terpiridina]-4′-carboxilato]

This compound was prepared following the same method described above using 1 mmol of trimethylsilyl-2,2′:6′,2″-terpyridine-4′-carboxylate (previously prepared) and 1 mmol of MoO_2Cl_2.

2.3.5 MoO_2[(S(+)-2-[(2-oxidopropyl)iminomethyl]-4-(((trimethylsilyl)oxy)carbonyl)phenolato-κ^3N,O,O′]

Molybdenum Schiff base complex was prepared following a modified methodology reported by Romanowski and, Kira [29]. 1 mmol of S-(+)-1-amino-2-propanol in methanol (10 mL) solution was added to 1 mmol of a trimethylsilyl-3-formyl-4-hydroxybenzoate in MeOH (10 mL) and heated with stirring under reflux for 1 h. $MoO_2(acac)_2$ (1 mmol) in MeOH (10 mL) was then added and stirred at room temperature for 2 h. After cooling, a precipitate separated and was filtered off, washed and recrystallized from MeOH.

2.3.6 MoO_2Ln Grafting Procedure

A benzene solution (50 mL) containing MoO_2(Ln-trimethylsilylated) was added to thoroughly dried (60 °C, 10–5 mbar, 24 h) TiO_2 nanotubes. The suspension was slowly stirred at 25 °C for 12 h, filtered, washed thoroughly with benzene (2 × 30 mL), and dried under vacuum to give the three catalytic systems shown in Fig. 2. The MoO_2Ln complexes grafted on TiO_2-NT were named as: $Mo^{(VI)}Cl_2O_2$(bipy)/TiO_2-NT (Fig. 2-1), $Mo^{(VI)}Cl_2O_2$(terpy)/TiO_2-NT (Fig. 2-2) and $Mo^{(VI)}O_2$(Schiff base)/TiO_2-NT (Fig. 2-3).

2.4 Limonene Photo-Oxidation

The oxidation of limonene with O_2 was performed in a 15 mL glass batch microreactor (ACEGLASS) equipped

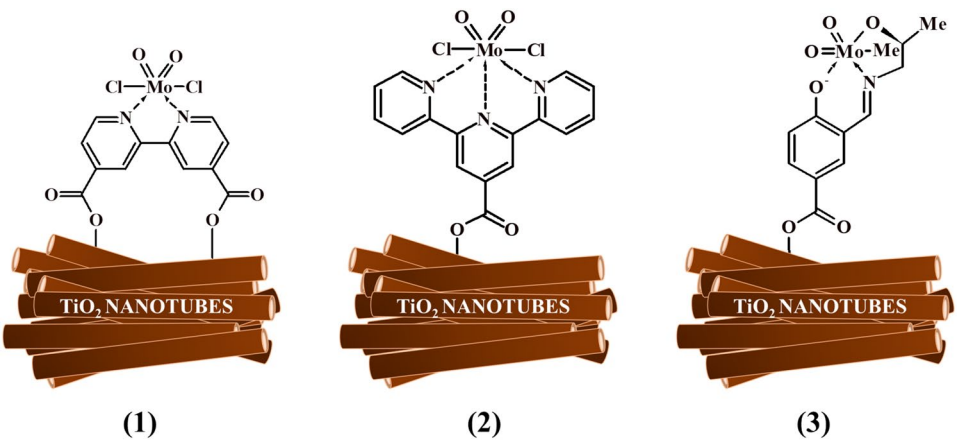

Fig. 2 Dioxo-Mo complexes with ligands bipyridine (**1**), terpyridine (**2**) and Schiff base (**3**) ligands anchored on TiO_2 nanotubes

with a mercury lamp (UV PenRay, λ = 360 nm). Typically, the reactor was loaded with 10 mL 1×10^{-2} M limonene solution in CH_3CN and 15 mg of catalyst and maintained under atmospheric pressure at 19 °C. The oxidation reaction under O_2 during 18 h was performed 3 times. Taking samples every 2 h and quantified by the standard internal method to control reaction progress was followed. Liquid samples were withdrawn, immediately filtered and analyzed by gas chromatography (GC-HP-6890) using a HP-INNO-WAX column (30 m × 0.32 mm × 0.25 µm) connected to a FID detector. Quantification of the products was performed using benzene as the internal standard. Reaction products were also identified by GC–MS with an Agilent Technologies 6890 Plus chromatograph (Palo Alto, CA, EE. UU.), equipped with a selective mass detector Agilent Technologies 5973N (EI, 70 eV, m/z 40–350) and a fused silica capillary column with 5% phenyl-poly(dimethylsiloxane) coating (DB-5 ms, J&W Scientific, Folsom, CA, EE. UU.) (60 m × 0.25 mm × 0.25 µm).

3 Results and Discussion

TiO_2 nanotubes (TNTs, Fig. S1 ESI) were prepared by an alkaline hydrothermal method and were fully characterized [25]. DRS spectra of TNTs allow confirming that absorption of this material is close to 380 nm. The choice of ligands (bipyridine, terpyridine, and Schiff base type) was made taking into account: (a) resistance against oxidation, (b) a straight-forward synthetic route, and (c) the possibility to change electronic and steric characteristics by simple variation of the starting materials [30]. FTIR spectra are shown in Fig. 3, evidence of the successful preparation and covalent anchoring onto the surface of TiO_2 nanotubes. $Mo^{(VI)}Cl_2O_2$(bipyridine)/TiO_2-NT infrared spectra indicated the asymmetric and symmetric stretching vibrations of the *cis*-MoO_2 group at 946 cm^{-1} and 915 cm^{-1}, respectively. The stretching vibration bands related to the carboxylate ligand were observed at 1722 cm^{-1} (C=O), 1267 cm^{-1} (asymmetric COO–), and 1128 cm^{-1} (symmetric COO–). The Ti-COO– linkage was identified by the 1396 cm^{-1} asymmetric and 1368 cm^{-1} symmetric scissor vibration modes [21–24].

The complex with terpyridine ligand was also characterized by infrared spectroscopy. The signals around 1566 and 1534 cm^{-1} correspond to the vibrations in the plane of the C=N and C=C bonds of the aromatic rings [31, 32]. Doublet at 948 and 909 cm^{-1}, corresponding to the asymmetric and symmetric vibrations of the MoO_2 unit. Infrared spectra of the complex with Schiff base ligand shown a strong peak at 1646 cm^{-1} characteristic of the C=N bond assigned to azomethine group. A peak at 1555 cm^{-1} attributed to C=C bonds of salicylaldehyde moiety. Asymmetric and symmetric COO– stretches have been found at 1278 and 1044 cm^{-1}. Likewise, spectra display two bands at 945 (asymmetric) and 912 cm^{-1} (symmetric) correspondings again to the MoO_2 unit [29, 33].

Additionally, infrared characterization of free ligands, silylated ligands, and homogeneous complexes MoO_2Ln is provided in Figs. S2, S3 and S4 (ESI). The redshift of the C=N ligand signal when it was reacting with the MoO_2 precursor, suggest the coordination of N to Mo.

MoO_2Ln complexes grafted on TiO_2-NT were also characterized by Raman spectroscopy (Fig. 4). Raman analysis provided additional evidence of the successful immobilization of the MoO_2Ln complex on the TiO_2 nanotubes. First, the characteristic anatase phase peaks were observed at 145 cm^{-1} (symmetric stretching vibration of O–Ti–O), 390 cm^{-1} (symmetric bending vibration of O–Ti–O), 509 cm^{-1} (antisymmetric bending vibration of O–Ti–O) and 632 cm^{-1}, corresponding to the $E_{g(1)}$, $B_{1g(1)}$, $(A_{1g} + B_{1g(2)})$ and $E_{g(2)}$ modes, respectively [34]. Next, in the supported complexes with bulkier ligands, the double

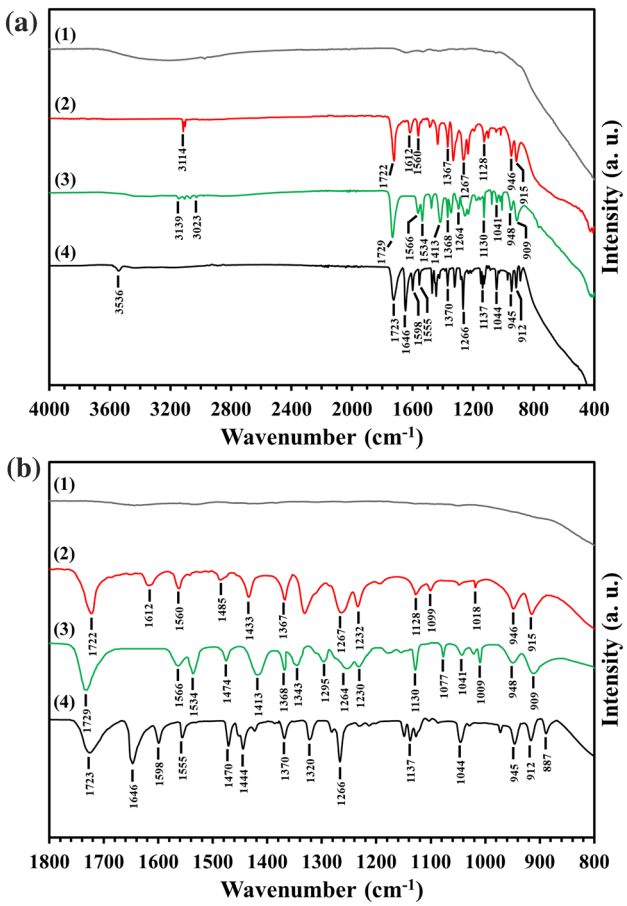

Fig. 3 **a** FT-IR spectra of (1): TiO_2-NT, (2): MoO_2Cl_2(bipyridine)/TiO_2-NT, (3): MoO_2Cl_2(terpyridine)/TiO_2-NT and (4): MoO_2(Schiff base)/TiO_2-NT, **b** zoom-in spectra between 1800 and 800 cm^{-1}

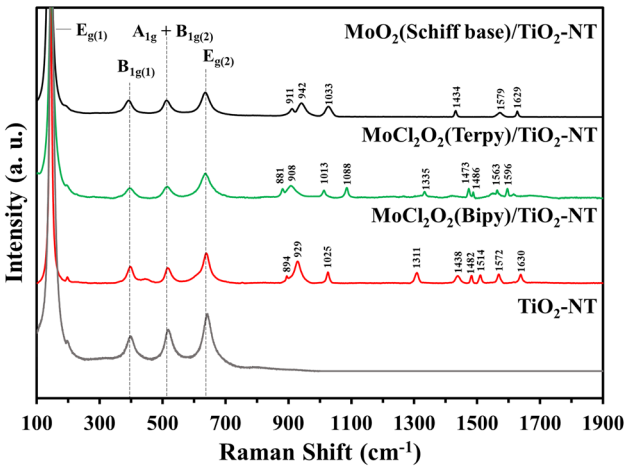

Fig. 4 Raman spectra of MoO_2Cl_2(bipyridine)/TiO_2-NT, MoO_2Cl_2(terpyridine)/TiO_2-NT and MoO_2(Schiff base)/TiO_2-NT

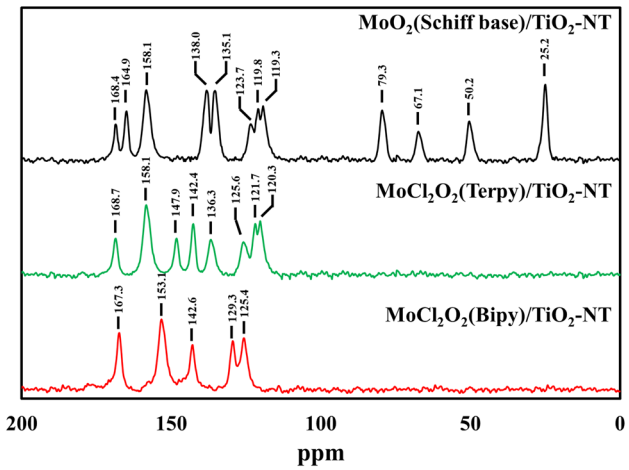

Fig. 5 ^{13}C CP-MAS NMR spectra of MoO_2Cl_2(bipyridine)/TiO_2-NT, MoO_2Cl_2(terpyridine)/TiO_2-NT and MoO_2(Schiff base)/TiO_2-NT

bands localized between 880 and 950 cm^{-1} correspond to $Mo(=O)_2$ group symmetrical and antisymmetric stretching [35]. $Mo^{(VI)}O_2Cl_2$(bipyridine)/TiO_2-NT system has a peak at 1025 cm^{-1} associated with "breathing" of the pyridine ring, at 1311, 1572, and 1630 cm^{-1} the signs of deformation are observed in the plane of the pyridine ring. Instead, peaks at 1438, 1482, and 1514 cm^{-1} are the signs of the deformations of the C–H bonds [36, 37]. $Mo^{(VI)}O_2$(Schiff base)/TiO_2-NT system has a signal at 1033 cm^{-1} corresponding to aromatic ring "breath," and three appreciable signals at 1434, 1579, and 1629 cm^{-1} of C–N, C=C and C=N [38] stretching vibrations characteristics of the azomethine. $Mo^{(VI)}O_2Cl_2$(terpyridine)/TiO_2-NT system presents the following signals: "breathing" pyridine rings at 1013 cm^{-1}, C–H flexion at 1088 cm^{-1} and 1335 cm^{-1}; C–C stretching inter-rings at 1473 and 1486 cm^{-1}; C=N stretching at 1563 and to C=C stretching at 1596 cm^{-1} [39].

^{13}C NMR spectra of all the molybdenum$^{(VI)}$ complexes were recorded in DMSO-d_6, and spectra of free ligands, silylated ligands, and homogenous complexes MoO_2Ln is provided in Figs. S5, S6 and S7 (ESI). The assignment of carbon signals was made based on their intensity, coupling patterns, and chemical shifts. Silylation was corroborated with the appearance of characteristic trimethylsilyl signal to high field. A significant chemical shift variation is observed, in particular, for the signals of the bipyridine and terpyridine rings carbons close to Mo center, after complexation with MoO_2Cl_2.

The covalent anchor of dioxo-Mo complexes on TNTs was corroborated by ^{13}C CP-MAS NMR (Fig. 5). All complexes show a characteristic peak between 167 and 168 ppm related to C(=O)–O–Ti^{4+} bound. The peaks corresponding to bipyridine and terpyridine ligands were detected between 120 and 160 ppm. In the case of Base Schiff ligand, the corresponding signals of C_8–C_{11} were detected between 20 and 80 ppm.

Additionally, the coordination of terpyridine ligand to Mo atom was confirmed through the characterization of the complex in solution. The NOESY spectrum of the free Mo complex (Fig. 6b) showed an NOE effect between protons H_3 and H_3' and H_5' and H_3''. This effect does not appear in the free ligand (Fig. 6a), which suggests

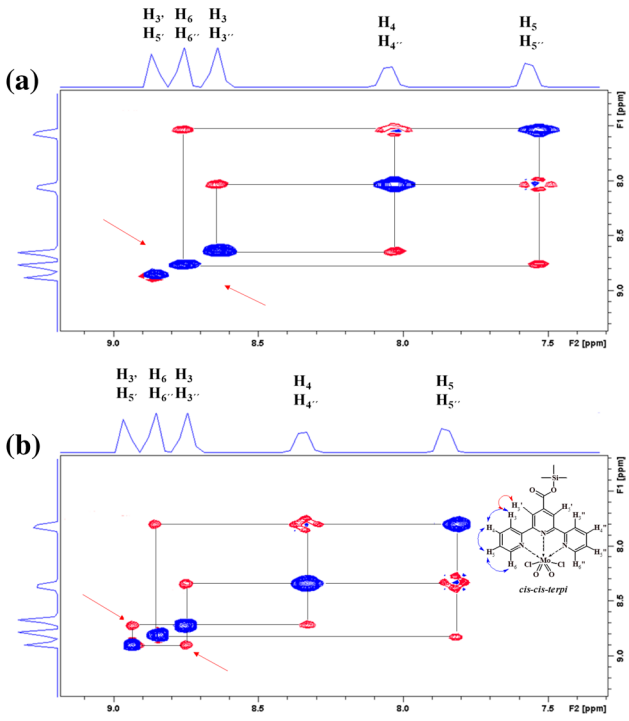

Fig. 6 NOESY spectrum of the terpyridine free ligand (**a**) and Mo–terpyridine complex (**b**)

coordination of terpyridine similar to those described by Bocian [40], type *cis–cis-* as seen in Fig. 5.

The N_2 adsorption–desorption isotherms of the parent nanotubes and modified Mo-based TiO_2-NT samples, and their corresponding pore size distributions are shown in Fig. 7. According to the IUPAC classification, the isotherm of the anatase nanotubes is of Type IVa, attributed to mesoporous materials. The observed H1-like hysteresis loop is characteristics of nanomaterials with uniform mesopores [41]. Compared to the pristine nanotubes, the three Mo-based TiO_2-NT samples also exhibit a Type IVa isotherm, but they show a more pronounced hysteresis loop. The nanotubes molybdenum modification procedure (dioxo-Mo grafting) causes hysteresis loops to be wider. The loops resemble more Type H2(b), indicating more complex pore structures in which network effects are important [41]. The specific surface areas, mean pore diameters and pore volumes of the TiO_2 samples before and after grafting of the dioxo-$Mo^{(VI)}$ complex are summarized in Table 1. The crystalline TiO_2 nanotubes exhibited a S_{BET} as high as 368 $m^2\ g^{-1}$ coupled to a high pore volume (0.90 $cm^3\ g^{-1}$). Such high values are attributed to the hollow tubular structure of the TiO_2-NT support, as already observed in the literature for various titania nanotubes (anatase phase) [27, 42, 43]. Both the internal side of the tubes and the nanotube ends contribute to the high BET surface area. Additionally, these anatase nanotubes are open at both ends, which makes the inner pore easily accessible. As expected, a decrease of pore volume and pore diameter was observed after the $Mo^{(VI)}$ immobilization step. Such decrease obviously results from the grafting of the dioxo-Mo complex on the walls of the titania nanotubes. Note that the dioxo-Mo grafted solids still exhibited a high specific surface area compared to the parent TiO_2-NT support (368 $m^2\ g^{-1}$).

Table 1 Textural properties of TiO_2-NT before and after $Mo^{(VI)}O_2Ln$ complex immobilization

Sample	S_{BET} ($m^2\ g^{-1}$)	V_p ($cm^3\ g^{-1}$)	D_p (nm)
TiO_2-NT	368	0.90	9.8
$MoCl_2O_2$(Bipy)/TiO_2-NT	346	0.67	7.9
$MoCl_2O_2$(Terpy)/TiO_2-NT	355	0.81	9.2
$MoCl_2O_2$(Schiff base)/TiO_2-NT	351	0.79	8.2

This textural proprieties modification is associated with functionalization on the inner walls of the TiO_2 nanotubes, see Fig. 7b. There was a greater decrease in pore diameter and volume in TiO_2 nanotubes modified with bipyridine ligand of dioxo-$Mo^{(VI)}$ complex. A lower diminution of NTTs textural properties with terpyridine ligand of the complex was observed. It indicates a possible functionalization only on the exterior wall of TiO_2 nanotubes.

The UV–Vis diffuse reflection spectrum observed the photo-absorption behavior of the MoO_2(Ln)/TiO_2-NT and shown in Fig. 8. The intraligand $\pi \rightarrow \pi^*$ transitions are sturdy and appear as very intense bands in the region 320–370 nm for ligands Schiff base and terpyridine [44, 45]. On the other hand, the low-energy absorptions recorded for all compounds between 500 and 600 nm are assigned to ligand-to-metal charge transfer (LMCT) transition arising between (phenolate-orbital π) and empty d orbital of the molybdenum atom.

The surface-bound complex was estimated with a loading of 1.20 mmol g^{-1} for MoO_2(bipyridine) complex, 0,

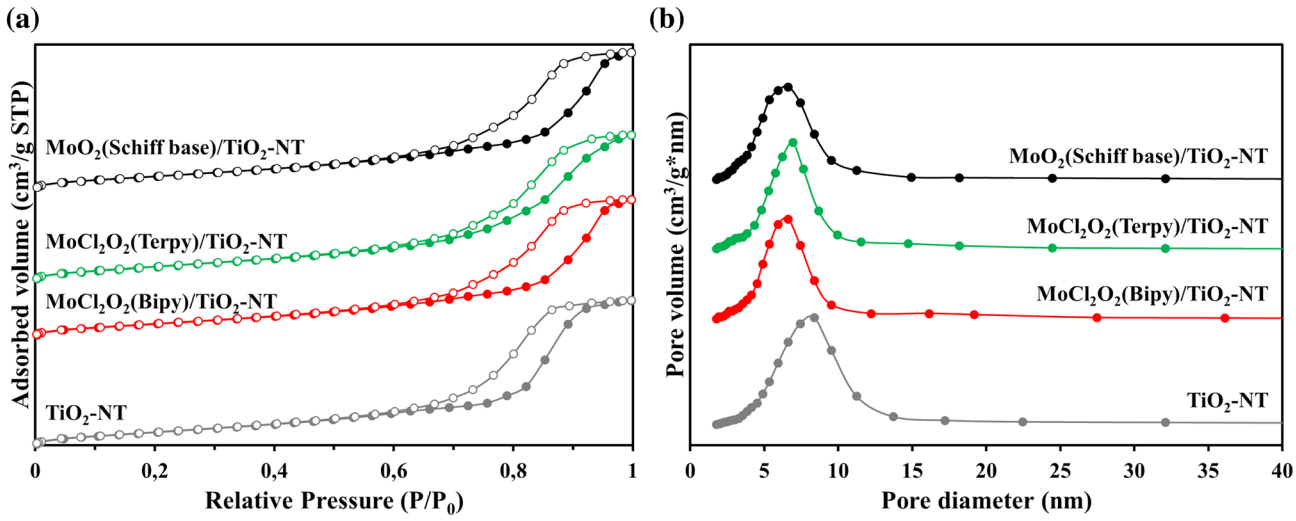

Fig. 7 **a** N_2 adsorption–desorption isotherms and **b** pore diameter distribution of TiO_2 nanotubes before and after modification with dioxo-$Mo^{(VI)}$ complexes

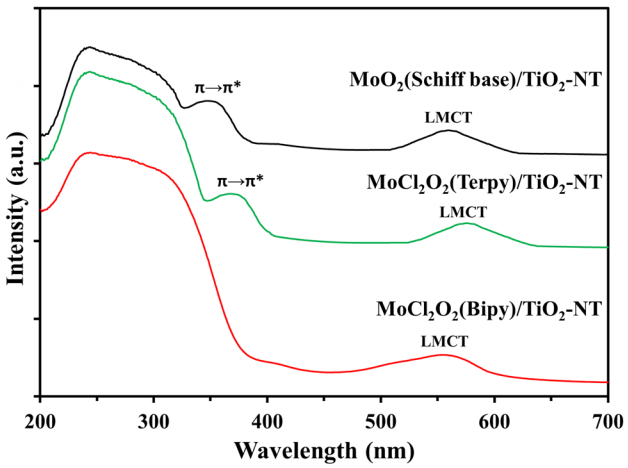

Fig. 8 UV–Vis diffuse reflection spectra of MoO_2Cl_2(Bipy)/TiO_2-NT, MoO_2Cl_2(Terpy)/TiO_2-NT and MoO_2(Schiff base)/TiO_2-NT

84 mmol g^{-1} for MoO_2(terpyridine), and 1.12 mmol g^{-1} for MoO_2(Schiff base) through Mo analysis by atomic absorption. Results were corroborated by TGA (Fig. S8 SI). In TGA analysis, three fundamental zones could be distinguished: one at a temperature below 150 °C, a stage in which water evaporates. Mass loss observed between 180 and 450 °C is associated with the loss of superficial hydroxyl groups. The third stage is between 450 and 650 °C whose loss of mass is related to the decomposition of the respective Mo complex. Formation of the complex was corroborated through C, H, and N elemental analysis before and after the grafting procedure. Elemental analysis of the supported $MoCl_2O_2$Bipy complex confirmed that molybdenum was stoichiometrically coordinated to the Bipy, Terpy and Schiff base ligands and the corresponding amount of Mo agreed with that quantified by atomic absorption spectrometry.

3.1 Selective Oxidation of (R)-(+)- and (S)-(−)-Limonene

3.1.1 Blank Reactions

In order to verify the photostimulated nature in OAT reaction, tests were carried out: (i) without light, (ii) without catalyst and (iii) with bare TiO_2-NT and light (all reactions were made in CH_3CN). Results were shown in Fig. 9 and Table 2. The reaction does not occur without light or catalyst. When bare TiO_2 nanotubes were used with light and O_2 conversion does not exceed 10% and selectivity was to products of allylic oxidation (carvone and carveol).

3.1.2 OAT to (R)-(+)-limonene and (S)-(−)-limonene

The catalytic activity of MoO_2Ln/TiO_2-NT catalysts was evaluated through the epoxidation reaction of (R)-(+)- and (S)-(−)-limonene with O_2 using UV–Vis radiation as promotor. Heterogeneous catalysts activity is determined by the amount of catalytically active sites and the degree of exposure of these active sites to the reactant. For this reason, selective epoxidation of (R)-(+)- and (S)-(−)-limonene was made with equimolar amounts of the dioxo-Mo complex anchored to TiO_2. Figure 9 shows the conversion of (a) (R)-(+)-limonene and (b) (S)-(−)-limonene with the three catalysts at 25 °C. The conversion of limonene increased with time and reached a maximum at 14 h. There is no apparent effect of the chiral center in limonene on the conversion. The OAT reactivity of the catalysts observed increases in order: MoO_2(Schiff base)/TiO_2-NT < $MoCl_2O_2$(bipyridine)/

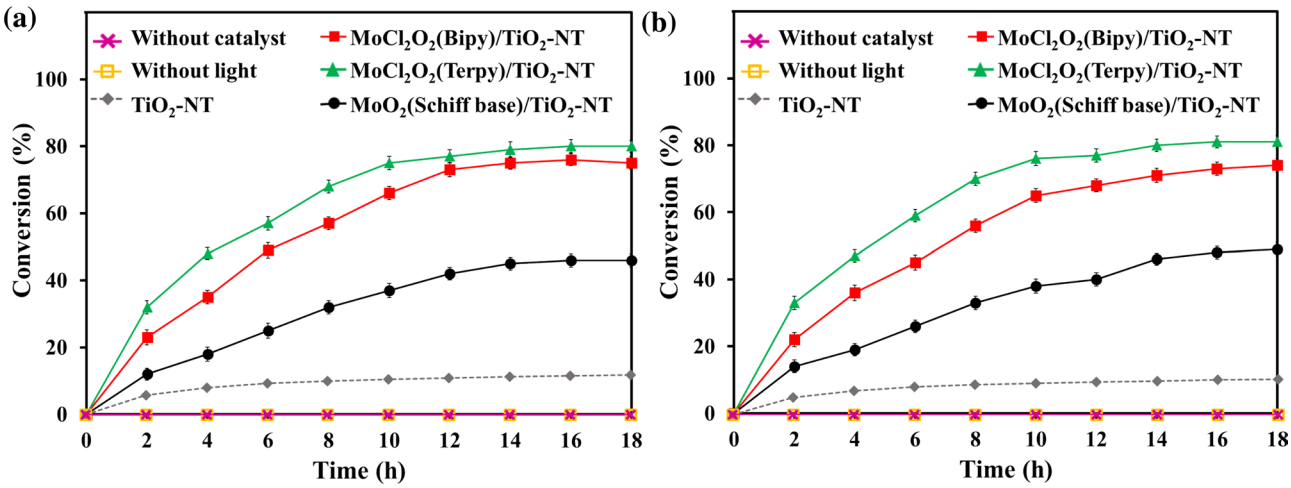

Fig. 9 Conversion (%) on time of **a** (R)-(+)-limonene and **b** (S)-(−)-limonene under different photocatalytic conditions and with different MoO_2Ln/TiO_2-NT systems

Table 2 Catalytic oxidation of (R)-(+)-limonene with O_2 under different reaction conditions after 18 h

Entry	Catalyst	Conditions	Conversion (%)	Selectivity (%)			
				1,2-Epoxide	Limonene diepoxide	Carvone	Carveol
1	Without catalyst	O_2, UV–Vis/25 °C	–	–		–	–
2	TiO_2-NT	O_2, without light/25 °C	–	–		–	–
3	TiO_2-NT	O_2, UV–Vis/25 °C	10	6	2	73	19
4	$MoCl_2O_2$(Bipy)/TiO_2-NT	O_2, UV–Vis/25 °C	75	83	10	7	–
5	$MoCl_2O_2$(Terpy)/TiO_2-NT	O_2, UV–Vis/25 °C	80	75	21	4	–
6	$MoCl_2O_2$(Schiff base)/TiO_2-NT	O_2, UV–Vis/25 °C	46	86	8	6	–

Reaction conditions: equimolar Mo quantities, [(R)-(+)-limonene] = 0.01 M, solvent: CH_3CN, reaction time: 18 h

TiO_2-NT < $MoCl_2O_2$(terpyridine)/TiO_2-NT. It observed a similar conversion of (R)-(+)-limonene and (b) (S)-(−)-limonene with the heterogeneous catalysts used at equimolar quantity. Results show that MoO_2Ln/TiO_2-NT catalysts are regioselective. In all cases 1,2-limonene oxide is the main product (selectivity > 84%, Table 2).

TiO_2 nanotubes are beneficial in photocatalysis because (1) larger specific surface area (up to 300 $m^2\ g^{-1}$) and pore volume (up to 1.00 $cm^3\ g^{-1}$); (2) ion-exchangeable ability; (3) remarkable and rapid long-distance electron-transport capability; and (4) enhanced light absorption due to the high ratio of length-to-tube diameter [46] Previously, we have observed that textural properties in nanotubes improve the photocatalytic activity with respect to other commercial and mesoporous TiO_2 supports using the same equimolar quantities dioxo-$Mo^{(VI)}$ complex grafted in TiO_2 in α-pinene oxidation [25].

During the reaction a synergistic effect was observed between: MoO_2Ln/TiO_2-NT and light. When TiO_2 is irradiated, a photogenerated electron flux from the semiconductor to Mo(VI) coordination sphere is generated evidencing a net increase in the rate of OAT [21–25]. In this process, the electron-rich (bipyridine, terpyridine or Schiff base) ligand functions acts as a bridge for the transit of electrons, see Scheme 1 (II). These electrons decrease the Mo=O bond order facilitating the oxygen atom transfer reaction. In the case of bare TiO_2 under UV light, an electron–hole pair is generated which, depending on the solvent used, will produce radicals that lead to the allylic oxidation of organic compounds as shown in the Scheme 1 (I). In this case, verbenone is the main oxidation product, along with verbenol. Such behavior could be tentatively explained by considering that the oxidation of limonene is caused by the photogenerated holes (directly or mediated by surface trapping) or by the attack of superoxide anions ($O_2^{-\cdot}$) and $HO^{\cdot}$ radicals generated by interfacial charge transfer. Although $HO^{\cdot}$ production is much lower in acetonitrile than in aqueous suspension, this mechanism may be invoked in the present conditions for TiO_2 suspensions, as already reported in the literature [47]. Then MoO_2Ln/TiO_2-NT will allow the selective oxidation of limonene through an OAT reaction stimulated by light.

Photostimulated OAT occurs in two steps, and a protocol has been previously implemented: O-atom transfer from dioxo-$Mo^{(VI)}$ to (R)-(+)-limonene under light, is reduced to $Mo^{(IV)}$. Reoxidation of $Mo^{(IV)}O$ by O_2 is produced in darkness: Fig. 10 and Scheme 2 [48]. The OAT process was examined for the oxidation of (R)-(+)-limonene with the $Mo^{(VI)}O_2Ln/TiO_2$-NT under inert N_2 atmosphere and light (step A). Then reoxidation of the catalyst is made in

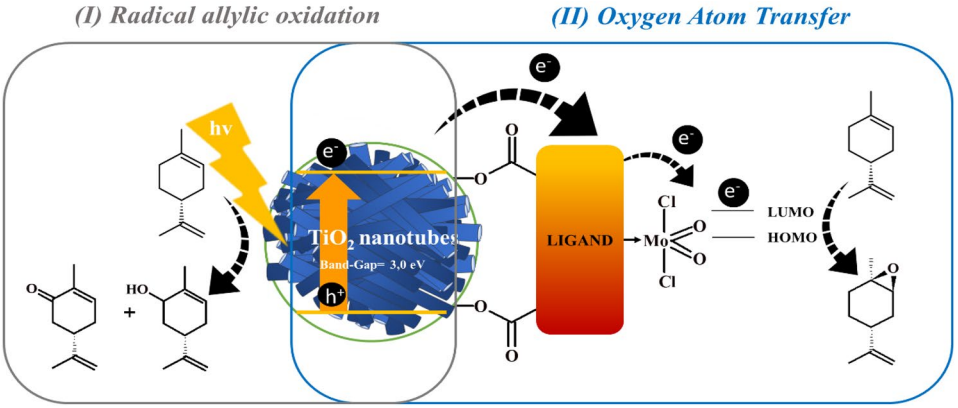

Scheme 1 Schematic representation of the photogenerated electron flux during irradiation of the $Mo^{(VI)}Cl_2O_2Bipy/TiO_2$-NT (II) and bare TiO_2 support (I)

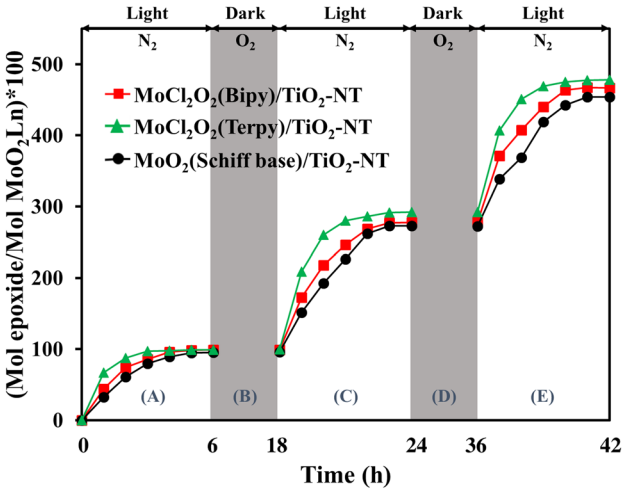

Fig. 10 (R)-(+)-limonene oxidation. Evolution of the [mol. α-pinene oxide]/[mol. MoO_2]) as a function of time in with the $Mo^{(VI)}O_2Ln/TiO_2$-NT catalysts: (A) light under N_2, (B) dark under O_2, (C) light under N_2, (D) dark under O_2, and (E) light under N_2

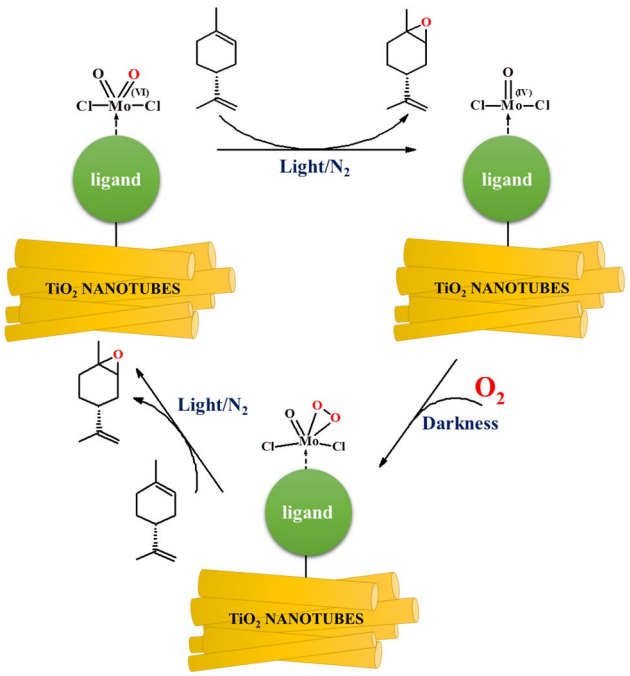

Scheme 2 Schematic representation of the photostimulated OAT process

under O_2 atmosphere without light (step B). In step A (N_2 atmosphere and UV–Vis), the $Mo(=O)_2$ complex donates one oxygen atom to the organic compound: OAT, the $Mo^{(VI)}$ is reduced to $Mo^{(IV)}$, and a vacant site is created. Then in step B (with O_2 and darkness), the $Mo{=}O^{(IV)}$ species are reoxidized by molecular oxygen to form an intermediary oxo–peroxo-$Mo^{(VI)}$ entity. After that under light, the O-atom transfer process permits the formation of 2 mol of the epoxide. These cycles sequence can be repeated.

In the first hours of the OAT reaction of (R)-(+)- and (S)-(−)-limonene, 1,2-epoxide was the main product, carvone and carveol were also detected in smaller quantities. For conversions above 20%, the formation of the diepoxide (1,2-), (8,9-) were also observed. This fact is following a decrease in selectivity to 1,2-limonene oxide at 4 h, as seen in Fig. 11. As limonene contains two double bonds, several epoxides may be formed. Here, the epoxidation of the electron-rich trisubstituted double bond (1,2-position) is favored as compared to the less electron-rich (more accessible) double bond in the 8,9-position. No formation of exocyclic epoxide (8,9-epoxide) suggests that limonene oxidation is regioselective to endocyclic epoxidation, and hence that limonene dioxide is formed by a subsequent epoxidation of 1,2-limonene oxide. In this case, 1,2-limonene oxide has a higher polarity compared to the parent limonene, which enables further epoxidation in the 8,9-position.

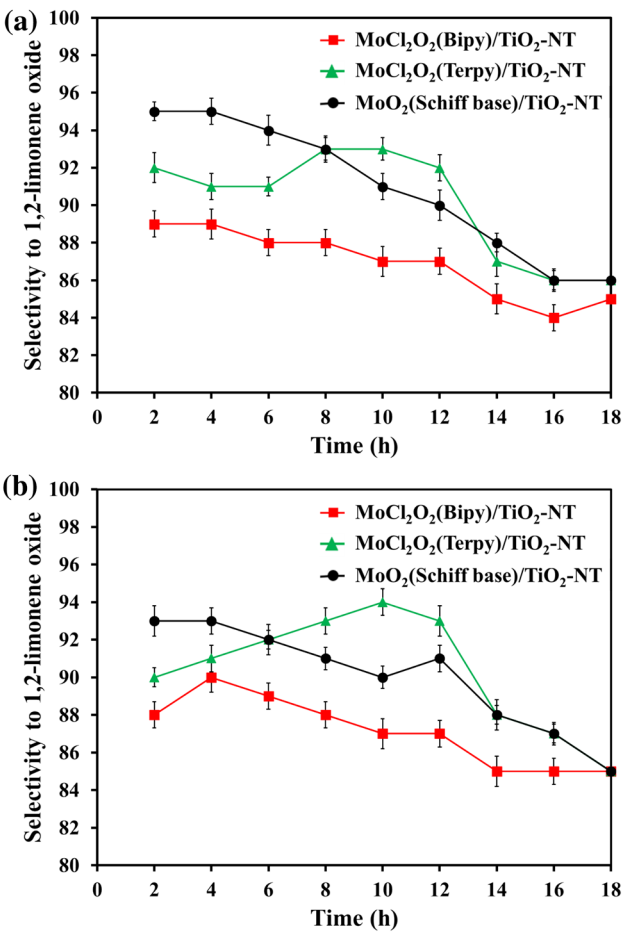

Fig. 11 Selectivity (%) towards the 1,2-limonene oxide using **a** (R)-limonene and **b** (S)-limonene

Most noteworthy is the significant diastereoselectivity observed, although the supported dioxo-$Mo^{(VI)}$ complex is not bearing any chiral ligand (Table 3; Fig. 12). The photo-stimulated OAT of (R)- and (S)-limonene with "non-chiral" dioxo$Mo^{(VI)}$ complexes immobilized displayed the formation of the *cis*-limonene-1,2-oxide as the main diastereoisomer. In the case of $Mo^{(VI)}Cl_2O_2$(bipyridine)/TiO_2-NT system, the epoxidation of the endocyclic double bond of (R)-(+)-limonene resulted in a diastereomeric excess (*d.e.*) of 36% of the isomer (1R, 2S, 4R)-(+)-*cis*-limonene-1,2-oxide (entry 1) concerning the (+)-*trans*-isomer. Starting from the (S)-(−)-limonene substrate, a *d.e.* of 34% was estimated for

Table 3 Epoxidation diastereoselectivity in (R)- and (S)-limonene with MoO_2Ln/TiO_2-NT systems at 18 h

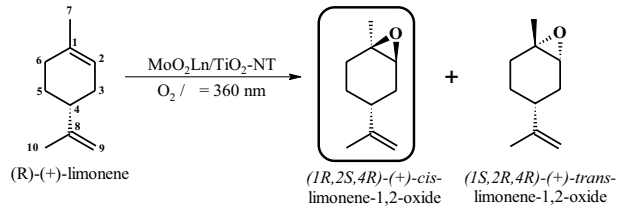

Entry	Catalyst	% d.e
1	$Mo^{(VI)}Cl_2O_2$(bipyridine)/TiO_2-NT	36
2	$Mo^{(VI)}Cl_2O_2$(terpyridine)/TiO_2-NT	35
3	$Mo^{(VI)}O_2$(Schiff base)/TiO_2-NT	16

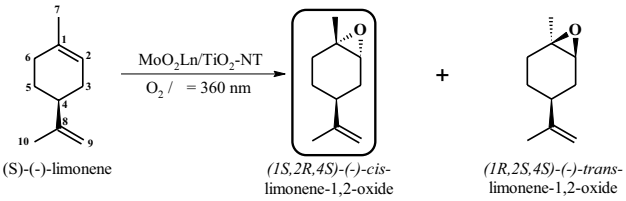

Entry	Catalyst	% d.e
4	$Mo^{(VI)}Cl_2O_2$(bipyridine)/TiO_2-NT	34
5	$Mo^{(VI)}Cl_2O_2$(terpyridine)/TiO_2-NT	33
6	$Mo^{(VI)}O_2$(Schiff base)/TiO_2-NT	52

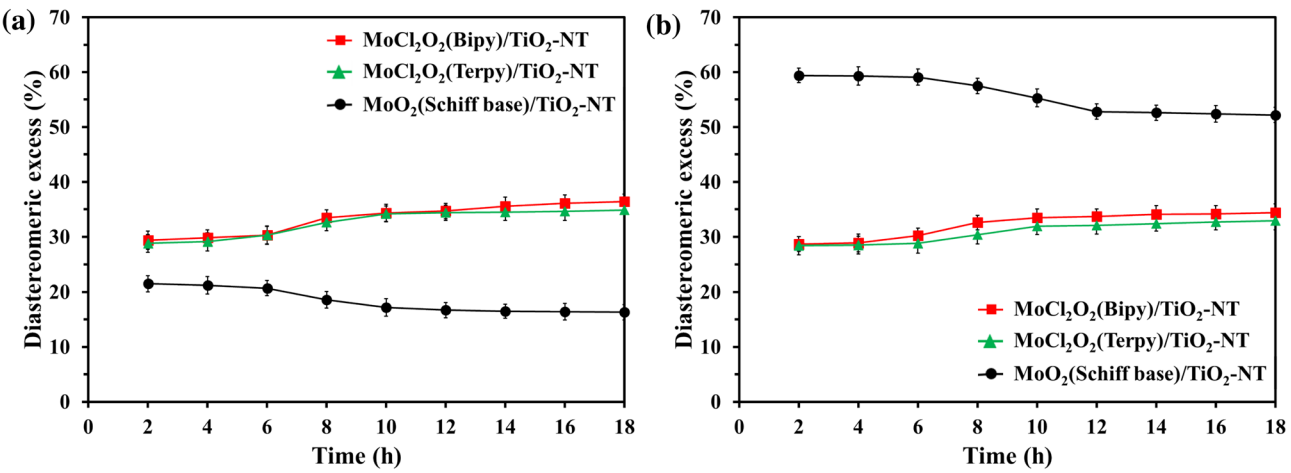

Fig. 12 Diastereomeric excess (%) evolution in time using **a** (R)-limonene and **b** (S)-limonene

the (1S, 2R, 4S)-(−)-*cis*-limonene-1,2-oxide isomer (entry 4). For $Mo^{(VI)}Cl_2O_2$(terpyridine)/TiO_2-NT system, (1R, 2S, 4R)-(+)-*cis*-limonene-1,2-oxide isomer was obtained with *d.e.* of 35% respect to the (+)-*trans*-isomer when (R)-(+)-limonene was used (entry 2). In the case of (S)-(−)-limonene, a *d.e.* of 33% was calculated for the (1S, 2R, 4S)-(−)-*cis*-limonene-1,2-oxide isomer (entry 5). In short, the anchored nonchiral dioxo-$Mo^{(VI)}$ complex does not present any chiral induction ability, suggesting that the chiral center in the (R)-(+)-and (S)-(−)-limonene is responsible for the formation of the diastereoisomer.

Nevertheless, photo-oxidation of (S)-(−)-limonene using a "chiral" (S) ligand like Schiff base of the catalyst gives rise to higher diastereoisomeric excess (52%, entry 6) with a matched pair. Whereas (S)-$Mo^{(VI)}O_2$(Schiff base)/TiO_2-NT with (R)-(+)-limonene generates a mismatched pair (entry 3). The corresponding diastereoisomeric excess are limited to 16%. This phenomenon has been described as a double asymmetric induction process [49]. It could be assuming a qualitative transition-state model proposed for trisubstituted olefins, where limonene interacts via a skewed side-on approach with the metal-oxo group of intermediary complex (Fig. 13). It is worth to note that the product stereochemistry is strongly dependent on the absolute configuration of $Mo^{(VI)}$ catalyst and limonene. In other words, not only the chiral catalyst center but also the chiral substrate center participates in the preferential formation of *cis*-limonene-1,2-oxide.

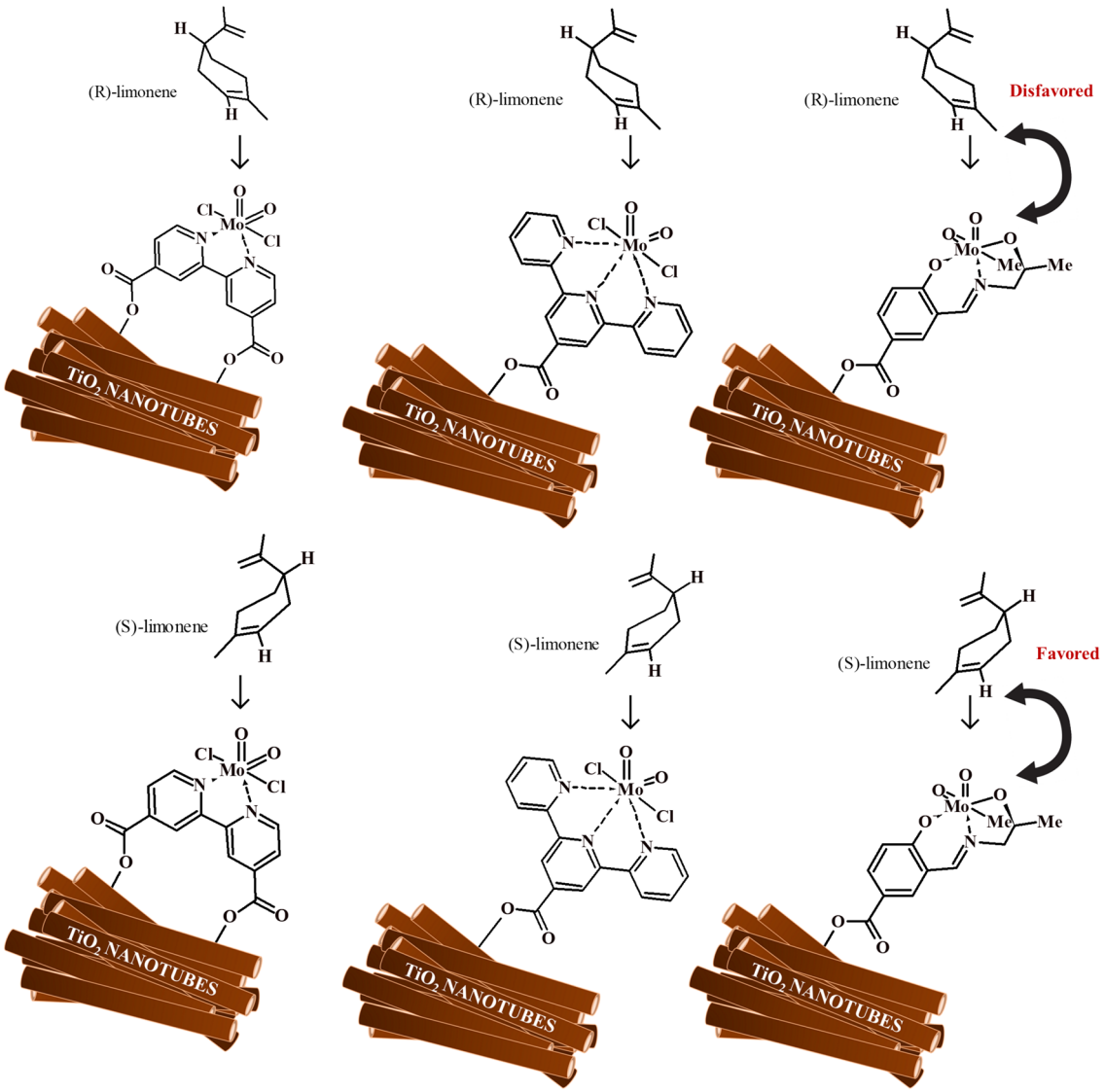

Fig. 13 Interaction of *chiral* and *non-chiral* $Mo^{(VI)}O_2$ active unit catalyst center with limonene 1,2-double bound

4 Conclusions

MoO_2Ln/TiO_2-NT systems under light drive the photostimulated OAT reaction permitting the selective oxidation of (R)-(+)- and (S)-(−)-limonene using O_2 as the primary oxidant agent. Selective epoxide formation is due to oxygen transfer from dioxo-$Mo^{(VI)}$ to (R)- or (S)-limonene stimulated by UV–Vis light. In darkness, the role of molecular oxygen is to reoxidize the [$Mo^{(IV)}$=O] unit and after that under light transfer oxygen again.

In the case of (R)- and (S)-limonene, the epoxidation of the electron-rich trisubstituted double bond (1,2-position) is favored as compared to the less electron-rich double bond in the 8,9-position. No formation of the exocyclic epoxide suggest that limonene oxidation is regioselective to endocyclic epoxidation. Specifically, all $Mo^{(VI)}O_2Ln/TiO_2$-NT catalysts showed high regioselectivity to 1,2-limonene oxide. Complexes with "non-chiral" bipyridine and terpyridine ligands showed moderate diastereoselectivity to *cis*-isomer. In contrast, complex with "chiral" Schiff base ligand showed an increase in diastereoisomeric excess (52%) due to a double asymmetric induction, the chiral catalyst center, and the chiral substrate center participate in the preferential formation of *cis*-limonene-1,2-oxide.

Acknowledgements We gratefully recognize the financial support by the Universidad Industrial de Santander—UIS (Project 1868). H. M. author is grateful to COLCIENCIAS (Doctorados Nacionales 647 Program) for the scholarship program. The authors thank Parque Tecnológico Guatiguará-UIS by physicochemical characterization analyzes.

Author Contributions All authors contributed equally to this work. HM prepared, characterized the catalysts, and performed the photo-catalytic measurements and interpretation. EP and FM designed the experiments and contributed to the interpretation of the experimental results. All authors read and approved the final manuscript.

Data Availability This work was presented to The 6th Latin-American Congress of Photocatalysis, Photochemistry and Photobiology LACP3, from 23 to 28 of September of 2019 at Bogota (https://www.utadeo.edu.co/en/lacp3-2019). The results are part of the thesis doctoral of HM but it is not realized public dissertation yet at the University of Industrial de Santander (https://www.uis.edu.co/webUIS/es/index.jsp).

Code Availability Not applicable for that section.

Compliance with Ethical Standards

Conflict of interest The authors declare that they have no conflicts of interest to reveal.

References

1. Brito JA, Royo B, Gómez M (2011) Catal.: an overview of chiral molybdenum complexes applied in enantioselective catalysis. Catal Sci Technol 1:1109–1118
2. Nodzewska A, Wadolowska A, Watkinson M (2019) Recent advances in the catalytic oxidation of alkene and alkane substrates using immobilized manganese complexes with nitrogen containing ligands. Coord Chem Rev 382:181–216
3. Michel T, Cokoja M, Sieber V, Kühn FE (2012) Selective epoxidation of (+)-limonene employing methyltrioxorhenium as catalyst. J Mol Catal A 358:159–165
4. Balcerzak L, Lipok J, Strub D, Lochynski S (2014) Biotransformations of monoterpenes by photoautotrophic micro-organisms. J Appl Microbiol 117:1523–1536
5. Cubillos J, Vargas M, Reyes J, Villa AL, Montes de Correa C (2010) Effect of the substrate and catalyst chirality on the diastereoselective epoxidation of Limonene using Jacobsen-type catalysts. Chirality 22:403–410
6. Cubillos J, Vásquez S, Montes de Correa C (2010) Salen manganese(III) complexes as catalysts for R-(+)-limonene oxidation. Appl Catal A 373:57–65
7. Młodzik J, Wróblewska A, Makuch E, Wróbel RJ, Michalkiewicz B (2016) Fe/EuroPh catalysts for limonene oxidation to 1,2-epoxylimonene, its diol, carveol, carvone and perillyl alcohol. Catal Today 268:111–120
8. Katsuki T (1995) Catalytic asymmetric oxidations using optically active (salen)manganese(III) complexes as catalysis. Coord Chem Rev 140:189–214
9. Ottenbacher RV, Samsonenko DG, Talsi EP, Bryliakov KP (2014) Highly enantioselective bioinspired epoxidation of electron-deficient olefins with H_2O_2 on aminopyridine Mn catalysts. ACS Catal 4:1599–1606
10. Águila S, Vazquez-Duhalt R, Tinoco R, Rivera M, Pecchi G, Alderete JB (2008) Stereoselective oxidation of R-(+)-limonene by chloroperoxidase from *Caldariomyces fumago*. Green Chem 10:647–653
11. Villa AL, Taborda F, Montes de Correa C (2002) Kinetics of limonene epoxidation by hydrogen peroxide on PW-Amberlite. J Mol Catal A 185:269–277
12. Oliveira P, Machado A, Ramos AM, Fonseca I, Braz Fernandes FM, Botelho do Rego AM, Vital J (2009) MCM-41 anchored manganese salen complexes as catalysts for limonene oxidation. Microporous Mesoporous Mater 120:432–440
13. Bhattacharjee S, Anderson JA (2004) Synthesis and characterization of novel chiral sulfonato-salen-manganese(III) complex in a zinc–aluminium LDH host. Chem Commun 554–555.
14. Saikia L, Srinivas D, Ratnasamy P (2006) Chemo-, regio- and stereo-selective aerial oxidation of limonene to the endo-1,2-epoxide over Mn(Salen)-sulfonated SBA-15. Appl Catal A 309:144–154
15. Bakhvalov OV, Fomenko VV, Salakhutdinov NF (2008) Modern methods for the epoxidation of α- and β-pinenes, 3-carene and limonene. Chem Sustain Dev 16:633–691
16. Tangestaninejad S, Mirkhani V (1998) Polystyrene-bound manganese(III) porphyrin as a heterogeneous catalyst for alkene epoxidation. J Chem Res S (12):788–789
17. Madadi S, Charbonneau L, Bergeron JY, Kaliaguine S (2020) Aerobic epoxidation of limonene using cobalt substituted mesoporous SBA-16 Part 1: optimization via Response Surface Methodology (RSM). Appl Catal B 260:118049–118062
18. Saraiva MS, Nunes CD, Nunes TG, Calhorda MJ (2013) Mo(II) complexes of 8-aminoquinoline and their immobilization in MCM-41. Appl Catal A 455:172–182
19. Brito JA, Ladeira S, Teuma E, Royo B, Gómez M (2011) Dioxomolybdenum(VI) complexes containing chiral oxazolines

applied in alkenes epoxidation in ionic liquids: a highly diastereoselective catalyst. Appl Catal A 398:88–95
20. Fernandes CI, Stenning GBG, Taylor JD, Nunes CD, Vaz PD (2015) Helical channel mesoporous materials with embedded magnetic iron nanoparticles: chiral recognition and implications in asymmetric olefin epoxidation. Adv Synth Catal 357:3127–3140
21. Páez CA, Castellanos NJ, Martínez F, Ziarelli F, Agrifoglio G, Páez-Mozo EA, Arzoumanian H (2008) Oxygen atom transfer photocatalyzed by molybdenum(VI) dioxodibromo-(4,4′-dicarboxylate-2,2′-bipyridine) anchored on TiO_2. Catal Today 133:619–624
22. Páez CA, Lozada O, Castellanos NJ, Martínez F, Ziarelli F, Agrifoglio G, Páez-Mozo EA, Arzoumanian H (2009) Arylalkane photooxidation under visible light and O_2 catalyzed by molybdenum(VI) dioxo-dibromo (4,4′-dicarboxylato-2,2′-bipyridine) anchored on TiO_2. J Mol Catal A 299:53–59
23. Castellanos NJ, Martínez F, Lynen F, Biswas S, Van Der Voort P, Arzoumanian H (2013) Dioxygen activation in photooxidation of diphenylmethane by a dioxomolybdenum(VI) complex anchored covalently onto mesoporous titania. Trans Met Chem 38:119–127
24. Martínez H, Cáceres MF, Martínez F, Páez-Mozo EA, Valange S, Castellanos NJ, Molina D, Barrault J, Arzoumanian H (2016) Photo-epoxidation of cyclohexene, cyclooctene and 1-octene with molecular oxygen catalyzed by dichloro dioxo-(4,4′-dicarboxylato-2,2′-bipyridine) molybdenum(VI) grafted on mesoporous TiO_2. J Mol Catal A 423:248–255
25. Martínez H, Amaya AA, Páez-Mozo EA, Martínez F (2018) Highly efficient epoxidation of α-pinene with O_2 photocatalyzed by dioxoMo(VI) complex anchored on TiO_2 nanotubes. Microporous Mesoporous Mater 265:202–210
26. Zwettler N, Judmaier ME, Strohmeier L, Belaj F, Mösch-Zanetti NC (2016) Oxygen activation and catalytic aerobic oxidation by Mo(IV)/(VI) complexes with functionalized iminophenolate ligands. Dalton Trans 45:14549–14560
27. Fen LB, Han TK, Nee NM, Ang BC, Johan MR (2011) Physicochemical properties of titania nanotubes synthesized via hydrothermal and annealing treatment. Appl Surf Sci 258:431–435
28. Arzoumanian H, Castellanos NJ, Martínez F, Paez-Mozo EA, Ziarelli F (2010) Silicon-assisted direct covalent grafting on metal oxide surfaces: synthesis and characterization of carboxylate *N*, *N*′-ligands on TiO_2. Eur J Inorg Chem 11:1633–1641
29. Romanowski G, Kira J (2016) Chiral molybdenum(VI) complexes with tridentate Schiff bases derived from S(+)-1-amino-2-propanol: synthesis, characterization and catalytic activity in the oxidation of prochiral sulfides and olefin. Polyhedron 117:352–358
30. Herrmann WA, Lobmaier GM, Priermeier T, Mattner MR, Scharbert B (1997) New dioxomolybdenum(VI) catalysts for the selective oxidation of terminal *n*-alkenes with molecular oxygen. J Mol Catal A 117:455–469
31. Castellucci E, Angeloni L (1979) IR and Raman spectra of a 2,2′-bipyridine single crystal: internal modes. Chem Phys 43:365–373
32. Niven ML, Percy GC (1978) The infrared spectra (3500–140 cm^{-1}) of the 2,2′-bipyridine, 2-aminomethylpyridine and ethylenediamine adducts and the sodium Tris-compounds of cobalt(II), nickel(II) and zinc(II) acetylacetonates. Trans Met Chem 3:267–271
33. Romanowski G, Kira J, Wera M (2018) Synthesis, structure, spectroscopic characterization and catalytic activity of chiral dioxidomolybdenum(VI) Schiff base complexes derived from R(−)-2-amino-1-propanol. Inorg Chim Acta 483:156–164
34. Hearne GR, Zhao J, Dawe AM, Pischedda V, Maaza M, Nieuwoudt MK, Kibasomba P (2004) Effect of grain size on structural transitions in anatase TiO_2: a Raman spectroscopy study at high pressure. Phys Rev 70:134102–134110
35. Sugimoto H, Harihara M, Shiro M, Sugimoto K, Tanaka K, Miyake H, Tsukube H (2005) Dioxo-molybdenum(VI) and mono-oxo-molybdenum(IV) complexes supported by new aliphatic dithiolene ligands: new models with weakened MoO bond characters for the arsenite oxidase active site. Inorg Chem 44:6386–6392
36. Brolo AG, Jiang Z, Irish DE (2003) The orientation of 2,2′-bipyridine adsorbed at a SERS-active Au(1 1 1) electrode surface. J Electroanal Chem 547:163–172
37. Castellucci E, Angeloni L, Neto N, Sbrana G (1979) IR and Raman spectra of a.2,2′-bipyridine single crystal: internal modes. Chem Phys 43:365–373
38. Heyde ME, Gill D, Kilponen RG, Rimai L (1971) Raman spectra of Schiff bases of retinal (models of visual photoreceptors). J Am Chem Soc 93:6766–6780
39. Sant'Ana AC, Alves WA, Santos RHA, Ferreira AMD, Temperini MLA (2003) The adsorption of 2,2′:6′,2″-terpyridine, 4′-(5-mercaptopentyl)-2,2′:6′,2″-terpyridinyl, and perchlorate on silver and copper surfaces monitored by SERS. Polyhedron 22:1673–1682
40. Bocian A, Brykczynska D, Kubicki M, Hnatejko Z, Walesa-Chorab M, Gorczynski A, Patroniak V (2019) Complexation behavior of 6,6″-dimethyl-2,2′:6′,2″-terpyridine ligand with Co(II), Au(III), Ag(I), Zn(II) and Cd(II) ions: synthesis, spectroscopic characterization and unusual structural motifs. Polyhedron 157:249–261
41. Thommes M, Kaneko K, Neimark AV, Oliver JP, Rodriguez-Reinero F, Rouquerol J, Sing KSW (2015) Physisorption of gases, with special reference to the evaluation of surface area and pore size distribution (IUPAC Technical Report). Pure Appl Chem 87:1051–1069
42. Bavykin DV, Parmon VN, Lapkin AA, Walsh FC (2004) The effect of hydrothermal conditions on the mesoporous structure of TiO_2 nanotubes. J Mater Chem 14:3370–3377
43. Ribbens S, Meynen V, Van Tendeloo G, Ke X, Mertens M, Maes BUW, Cool P, Vansant EF (2008) Development of photocatalytic efficient Ti-based nanotubes and nanoribbons by conventional and microwave assisted synthesis strategies. Microporous Mesoporous Mater 114:401–409
44. Romanowski G, Kira J (2017) Synthesis, characterization and catalytic activity of dioxidomolybdenum(VI) complexes with tridentate Schiff bases derived from 1R, 2S(−)-norephedrine. Polyhedron 134:50–58
45. Wu ZY, Wang W (2015) Terpyridine chelate complex-functionalized single-walled carbon nanotubes: synthesis and redox properties. Fullerenes Nanotubes Carbon Nanostruct 23:131–141
46. Liu N, Chen X, Zhang J, Schwank JW (2014) A review on TiO_2-based nanotubes synthesized via hydrothermal method: formation mechanism, structure modification, and photocatalytic applications. Catal Today 225:34–51
47. Ciriminna R, Parrino F, De Pasquale C, Palmisano L, Pagliaro M (2018) Photocatalytic partial oxidation of limonene to 1,2 limonene oxide. Chem Commun 54:1008–1011
48. Judmaier ME, Holzer C, Volpe M, Mösch-Zanetti NC (2012) Molybdenum(VI) dioxo complexes employing Schiff base ligands with an intramolecular donor for highly selective olefin epoxidation. Inorg Chem 51:9956–9966
49. Masamme S, Choy W, Petersen JS, Sita LR (1985) Double asymmetric synthesis and a new strategy for stereochemical control in organic synthesis. Angew Chem Int Ed Engl 24:1–30

Affiliations

Henry Martínez Q.[1] · Edgar A. Paez-Mozo[1] · Fernando Martínez O.[1]

[1] Centro de Investigaciones en Catálisis – CICAT, Escuela de Química, Universidad Industrial de Santander, Km. 2 vía El Refugio, Piedecuesta, Colombia